An affinity-based scoring scheme for predicting DNA-binding activities of modularly assembled zinc-finger proteins

506–515 *Nucleic Acids Research, 2009, Vol. 37, No. 2* *Published online 4 December 2008*
doi:10.1093/nar/gkn962

An affinity-based scoring scheme for predicting DNA-binding activities of modularly assembled zinc-finger proteins

Jeffry D. Sander[1,*], Peter Zaback[1], J. Keith Joung[2,3], Daniel F. Voytas[4] and Drena Dobbs[1,*]

[1]Department of Genetics, Development and Cell Biology, Bioinformatics and Computational Biology Program, Iowa State University, Ames, IA 50011, [2]Molecular Pathology Unit, Center for Cancer Research, and Center for Computational and Integrative Biology, Massachusetts General Hospital, 149 13th Street, Charlestown, MA 02129, [3]Department of Pathology, Harvard Medical School, Boston, MA 02115 and [4]Department of Genetics, Cell Biology and Development and Center for Genome Engineering, University of Minnesota, MN 55455, USA

Received August 7, 2008; Revised November 10, 2008; Accepted November 12, 2008

ABSTRACT

Zinc-finger proteins (ZFPs) have long been recognized for their potential to manipulate genetic information because they can be engineered to bind novel DNA targets. Individual zinc-finger domains (ZFDs) bind specific DNA triplet sequences; their apparent modularity has led some groups to propose methods that allow virtually any desired DNA motif to be targeted *in vitro*. In practice, however, ZFPs engineered using this 'modular assembly' approach do not always function well *in vivo.* Here we report a modular assembly scoring strategy that both identifies combinations of modules least likely to function efficiently *in vivo* and provides accurate estimates of their relative binding affinities *in vitro*. Predicted binding affinities for 53 'three-finger' ZFPs, computed based on energy contributions of the constituent modules, were highly correlated ($r = 0.80$) with activity levels measured in bacterial two-hybrid assays. Moreover, K_d values for seven modularly assembled ZFPs and their intended targets, measured using fluorescence anisotropy, were also highly correlated with predictions ($r = 0.91$). We propose that success rates for ZFP modular assembly can be significantly improved by exploiting the score-based strategy described here.

INTRODUCTION

The ability to reliably engineer DNA binding proteins that recognize any desired DNA sequence would provide an unprecedented level of control over genetic information; for example, by allowing the creation of site-specific nucleases that specifically alter genomic DNA (1–5). The C_2H_2 zinc-finger domain (ZFD) is arguably the best characterized DNA binding motif and offers considerable promise for the rational engineering of site-specific DNA binding proteins (6–11). Zinc-finger proteins (ZFPs) consist of multiple individual ZFDs, each of which typically recognizes adjacent sequence triplets in duplex DNA (Figure 1). An individual ZFD comprises a pair of antiparallel β-strands and one α-helix, which coordinate a zinc ion through conserved pairs of cysteine and histidine residues. In the canonical three-finger domain of the Zif268 transcription factor, the amino acid side chains at positions −1, +3 and +6 relative to the amino-terminal end of the α-helix typically make base-specific contacts with three adjacent nucleotides within the major groove of double-stranded DNA (12). An aspartic acid residue in the +2 position of the DNA recognition helix can specify a fourth nucleotide, resulting in either target-site overlap with an adjacent module or specification of an additional nucleotide at the 3′-end of the target site (13,14).

Several research groups have characterized ZFDs that recognize many of the 64 possible DNA triplets (15–20). Using a 'modular assembly' approach, novel ZFPs that recognize variant DNA sites are assembled by simply

*To whom correspondence should be addressed. Tel: +1 515 294 4991; Fax: +1 515 294 6790; Email: jdsander@iastate.edu
Correspondence may also be addressed to Drena Dobbs. Tel: +1 515 294 4991; Fax: +1 515 294 6790; Email: ddobbs@iastate.edu

The authors wish it to be known that, in their opinion, the first two authors should be regarded as joint First Authors.

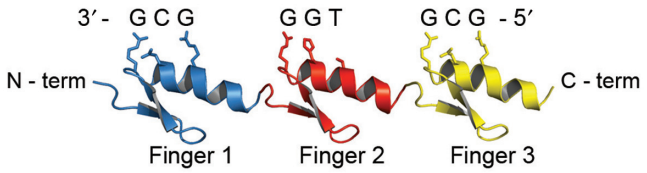

Figure 1. A three-finger ZFP with its DNA target site. A ZFP consisting of three adjacent ZFDs binds its target DNA through contacts between the amino acids of the DNA recognition helices and consecutive nucleotides in the DNA. The protein chain is drawn in the N- to C-terminal direction and the DNA target in the 3′–5′ direction. Note that an 'unnatural' extended array is shown to better illustrate the critical amino acid/nucleotide contacts. Structure diagrams were generated using PyMol (http://www.pymol.org).

stringing together individual ZFDs. In practice, however, ZFPs made by modular assembly display a wide range of binding affinities and specificities (15,19,21–23). Although modular assembly has proven useful for some *in vivo* applications, such as artificial transcription factors, recent work suggests that the success rate of creating artificial zinc-finger nucleases (ZFNs–fusions of engineered zinc fingers to a non-specific nuclease domain) by this method is considerably lower (24,25). These low success rates, together with the inability to predict which ZFPs are likely to function *in vivo*, have motivated our groups to improve the procedures and design criteria for ZFP engineering (25,26).

The present study was motivated by our observation that among a small set of modularly assembled ZFPs, those that fail to function *in vivo* are more likely to possess modules previously shown to have relatively low affinity for target DNA. This observation implies that insufficient affinity can contribute to poor function *in vivo* and also suggested that it might be possible to predict the affinity of a modularly assembled ZFP using existing affinity data for component modules. Here we test these hypotheses and demonstrate that both the *in vitro* binding affinity and the lack of *in vivo* activity of a ZFP can be predicted using the energy contributions of its component ZFDs. Our approach for predicting the binding of ZFPs to desired target sequences should improve success rates of modular assembly by guiding investigators away from target sites and ZFP combinations least likely to function *in vivo*.

MATERIALS AND METHODS

Zinc-finger modules and three-finger arrays (ZFPs)

All ZFDs used in these experiments have been described by the Barbas group (15) and are referred to as 'Barbas modules'. ZFPs containing desired three-finger (three-module) arrays were assembled by iterative ligation and cloning of restriction fragments encoding ZFDs using reagents and protocols previously described by the Zinc Finger Consortium (http://www.zincfingers.org/) (27). ZFP-encoding fragments were then cloned into vectors for expression as Gal11P-hybrid proteins in the bacterial two-hybrid (B2H) system as previously described (27).

B2H assays

A series of B2H reporter plasmids, each harboring a target binding site for one of 27 different three-finger ZFPs, was constructed by cloning synthetic target oligonucleotides into reporter plasmid pBAC-lacZ as previously described (27). Binding of a Gal11P-ZFP hybrid protein to the target sequence on a B2H reporter plasmid triggers transcriptional activation of a *lacZ* reporter gene encoding β-galactosidase. *In vivo* ZFP performance was therefore assayed using a β-galactosidase assay in which ZFP-induced activation of *lacZ* expression was measured relative to control constructs lacking the ZFP.

Zinc finger–maltose binding protein fusion protein construction, expression and purification

Zinc finger–maltose binding protein (MBP) fusion protein constructs were generated by transferring three-finger arrays, assembled as described above, into pHMTC (28). The MBP fusion plasmids were transformed into BL21 *Escherichia coli* cells (Invitrogen) using standard chemical transformation procedures (29).

For protein expression, 5 ml cultures were grown for 16 h at 30°C with agitation in ZFE broth [Luria Broth (LB), 1.11 mM dextrose, 100 μg/ml ampicillin]. Expansion cultures of 10 ml were inoculated from these overnight cultures (1:100 dilution) and grown to an OD_{600} of 0.5 before a 2 h induction with isopropyl β-D-1-thiogalactopyranoside (IPTG). Cells were harvested by centrifugation for 10 min at 4000*g* at 4°C and frozen overnight at −20°C. The following day, cells were resuspended in 4 ml WB1 (15 mM HEPES pH 7.8, 200 mM NaCl, 20 μM $ZnSO_4$)/1 mM PMSF/0.1% Nonidet™ P40 (NP-40) and refrozen at −70°C. Cells were then thawed in ice water and centrifuged at 9000*g* at 4°C for 20 min. To remove remaining nucleic acids, the resulting supernatant was transferred to a new cold tube and polyethyleneimine was added to 0.1%. The supernatant was then incubated for 30 min before a second centrifugation at 16 000 *g* at 4°C for 30 min.

Amylose beads (NEB) were prepared in 50 μl aliquots in 1.5 ml micro-centrifuge tubes according to manufacturer's instructions. Beads were washed (suspended, spun down and supernatant removed) three times in 1 ml WB1/0.1% NP-40 at 4°C and resuspended in 450 μl WB1. For affinity purification, 1 ml of clarified protein supernatant was added to prepared beads, and incubated at 4°C for 30 min. The slurry was centrifuged and the supernatant was removed. The proteins bound to beads were washed two times with 700 μl WB1/0.1% NP-40 and two times with zinc buffer A (ZBA; 10 mM Tris–HCl, pH 7.5, 90 mM KCl, 1 mM $MgCl_2$, 90 μM $ZnCl_2$)/0.1% NP-40 (15). Purified proteins were then eluted in 200 μl ZBA/0.1% NP-40/40 mM maltose for 30 min at room temperature, with gentle agitation. After elution, beads were centrifuged at 16 000*g*. The supernatant was transferred to a new cold tube and centrifuged again at 16 000*g*. The supernatant was transferred to a new cold tube and gently stirred to mix protein. Proteins were stored at −70°C in Axygen MaxymumRecovery™ tubes. Protein concentrations were estimated using a Bradford assay against a

bovine serum albumin (BSA) standard in ZBA/0.1% NP-40.

Binding measurements using fluorescence anisotropy

Binding reactions were performed in ZBA/0.1% NP-40/0.1 mg/ml non-acetylated BSA (Sigma) for 30 min on ice with 5 nM target DNA. Target sites (shown in Figure 2a) were formed using hairpin DNA oligonucleotides as described (15). HPLC purified, 3′-6-FAM-labeled oligonucleotides were ordered from Integrated DNA Technologies (Coralville, IA, USA). In each experiment, two serial dilutions of purified ZFP-MBP fusion protein were performed over a range of 1000–0.122 nM. Reported binding affinity values are based on the average of three separate binding experiments, performed on different days, using three separate protein preparations. Fluorescence anisotropy (FA) measurements were made using a Varian Cary Eclipse spectrophotometer in L-format configuration. Each value was based on five measurements averaged over 5 s, using a 490 nm excitation wavelength (5 nm slit width), and 530 nm emission wavelength (20 nm slit width) at 880 V. Background light scattering for each protein sample dilution was measured and subtracted to correct for protein concentration-dependent variation in intensities. K_d values were determined by nonlinear regression (30,31) using Prism (http://www.graphpad.com/prism/Prism.htm).

RESULTS

To test the hypothesis that binding energy contributions of individual ZFDs can be used to predict the *in vitro* binding affinities and *in vivo* performance of extended ZFP arrays, 27 three-module ZFPs were constructed by assembling various GNN-specific modules previously characterized by the Barbas group (15). ZFP compositions were chosen to systematically explore a wide range of predicted binding affinities and to test the influence of context on module performance. As shown in Table 1, ZFDs were divided into three affinity classes based on their reported affinity constants measured in a fixed context, namely as fingers in the middle position of a three-finger Zif268 variant (15). Modules comprising Zif268 variants with K_d values <10 nM were categorized as 'strong', K_d = 10–30 nM as 'moderate' and $K_d > 30$ nM as 'weak' (Table 1). Using three different modules to represent each binding class, all possible combinations of strong, moderate and weak affinity modules for a three-module ZFP were assembled. To allow direct comparisons among proteins that differ by a single module, ZFPs were designed in subgroups in which only one finger position was varied (Table 2).

Predicting relative binding energies for modularly designed ZFPs

If one assumes that the binding energy of a three-finger ZFP (ΔG°_{ZFP}) is equal to the sum of the binding energies of its three component ZFDs (ΔG°_{ZFD}) [Equation (1)], it follows that the difference in binding energy between any two ZFPs is the sum over the positions of the difference in binding energy between the modules at each position [Equation (2)].

$$\Delta G^\circ_{ZFP} = \Delta G^\circ_{ZFD1} + \Delta G^\circ_{ZFD2} + \Delta G^\circ_{ZFD3} \quad (1)$$

$$\begin{aligned}\Delta\Delta G_{ZFP1-ZFP2} = &\left(\Delta G^\circ_{ZFP1-F1} - \Delta G^\circ_{ZFP2-F1}\right)\\ &+ \left(\Delta G^\circ_{ZFP1-F2} - \Delta G^\circ_{ZFP2-F2}\right)\\ &+ \left(\Delta G^\circ_{ZFP1-F3} - \Delta G^\circ_{ZFP2-F3}\right)\end{aligned} \quad (2)$$

Because the ZFDs used in this study were evaluated in the middle (F2) position of a three-finger ZFP, and because the other fingers (F1 and F3) were constant in all these ZFPs, the differences in measured binding constants among these constructs should be attributable to the differences in binding energy between the F2 ZFDs. Thus, $\Delta\Delta G$ can be calculated between any two ZFDs by using the identity relating Gibbs free energy to K_d [Equation (3), RT = 0.58].

$$\Delta G^\circ_{ZFD1} - \Delta G^\circ_{ZFD2} = -RT\ln(K_{dZFP1}/K_{dZFP2}) \quad (3)$$

To compare binding affinity measurements with predicted values, the predicted $\Delta\Delta G$ was calculated as the difference between each ZFP and a standard (STD) ZFP composed entirely of the F2 domain of parental C7 (15).

$$\begin{aligned}\Delta\Delta G_{ZFD1} = -RT(&\ln(K_{dZFP1}/K_{dSTD})\\ &+ \ln(K_{dZFP2}/K_{dSTD})\\ &+ \ln(K_{dZFP3}/K_{dSTD}))\end{aligned} \quad (4)$$

Thus, using Equation (4) and binding constants for ZFP variants published by the Barbas group (15), we predicted $\Delta\Delta G$ values for 27 novel modularly assembled ZFPs constructed using Barbas GNN modules (Figure 2). Predicted $\Delta\Delta G$ values ranged from 2.1 kcal/mol for ZFP #1, containing three strong modules to 8.2 kcal/mol for ZFP #27 containing three weak modules.

In vivo activities of ZFPs are highly correlated with predicted binding energies

To evaluate *in vivo* binding of the 27 modularly assembled ZFPs to their cognate DNA targets, we used a quantitative B2H assay (32). In this assay, binding of a ZFP to its target site activates transcription of a *lacZ* reporter positioned downstream of an adjacent promoter. Thus, ZFP DNA-binding activity can be assessed by quantifying β-galactosidase activity in ZFP-expressing cells relative to control cells that do not express the ZFP. We chose to use the B2H system as an assay because recently published studies have shown that absence of ZFP activity in this system is an excellent predictor for failure of these proteins to function as ZFNs in human cells (24–26). For 25 of the 27 ZFPs tested, the level of *lacZ* activation observed was in excellent agreement with predicted energies (Figure 2a). Expression of the two ZFPs with the strongest predicted binding energy was toxic to cells,

(a)

ZFP#	Recognition Helix Sequences F1	F2	F3	Target DNA Sequence (5' – 3')	Predicted ΔΔ G	B2H Fold Activation (Avg.)	SEM
1*	TSGSLVR	RSDNLVR	RSDNLVR	GAGGAGGTT	2.15	Toxic	N/A
4	TSGNLVR	TSGHLVR	RSDNLVR	GAGGGTGAT	3.43	Toxic	N/A
7	RSDNLVR	DPGHLVR	TSGNLVR	GATGGCGAG	4.00	3.11	0.70
19*	DPGHLVR	TSGNLVR	RSDNLVR	GAGGATGGC	4.00	3.58	0.56
2*	TSGSLVR	RSDNLVR	QSSSLVR	GTAGAGGTT	4.02	4.88	0.62
3*	TSGSLVR	RSDNLVR	DPGHLVR	GGCGAGGTT	4.29	3.51	0.38
10	RSDELVR	TSGSLVR	TSGSLVR	GTTGTTGTG	4.66	1.77	0.09
8	RSDNLVR	DPGALVR	TSGHLVR	GGTGTCGAG	4.93	2.59	0.23
5	TSGNLVR	TSGHLVR	RSDELVR	GTGGGTGAT	5.00	1.74	0.15
11*	RSDELVR	TSGSLVR	RSDELVR	GTGGTTGTG	5.30	1.89	0.24
6	TSGNLVR	TSGHLVR	DPGHLVR	GGCGGTGAT	5.57	1.41	0.08
13*	RSDELVR	QSSSLVR	TSGSLVR	GTTGTAGTG	5.60	2.19	0.17
9	RSDNLVR	TSGELVR	DPGALVR	GTCGCTGAG	5.79	2.47	0.37
16	QSSSLVR	DPGHLVR	TSGNLVR	GATGGCGTA	5.87	1.88	0.47
20*	DPGHLVR	TSGNLVR	QSSSLVR	GTAGATGGC	5.87	3.09	0.21
22	DPGALVR	RSDELVR	TSGSLVR	GTTGTGGTC	5.87	1.95	0.08
12	TSGHLVR	TSGSLVR	TSGELVR	GCTGTTGGT	6.15	1.43	0.10
14	RSDELVR	QSSSLVR	RSDELVR	GTGGTAGTG	6.24	2.81	0.19
21*	DPGHLVR	TSGNLVR	TSGELVR	GCTGATGGC	6.43	0.92	0.04
25	TSGELVR	DPGHLVR	TSGNLVR	GATGGCGCT	6.43	1.54	0.20
17	QSSSLVR	DPGALVR	TSGHLVR	GGTGTCGTA	6.81	1.69	0.08
23	DPGALVR	RSDELVR	QSSSLVR	GTAGTGGTC	6.81	1.69	0.05
15	TSGHLVR	QSSSLVR	TSGELVR	GCTGTAGGT	7.09	1.96	0.21
24	DPGALVR	RSDELVR	TSGELVR	GCTGTGGTC	7.36	1.23	0.08
26	TSGELVR	DPGALVR	TSGHLVR	GGTGTCGCT	7.36	1.59	0.39
18	QSSSLVR	TSGELVR	DPGALVR	GTCGCTGTA	7.66	1.85	0.20
27*	TSGELVR	TSGELVR	DPGALVR	GTCGCTGCT	8.22	1.71	0.12

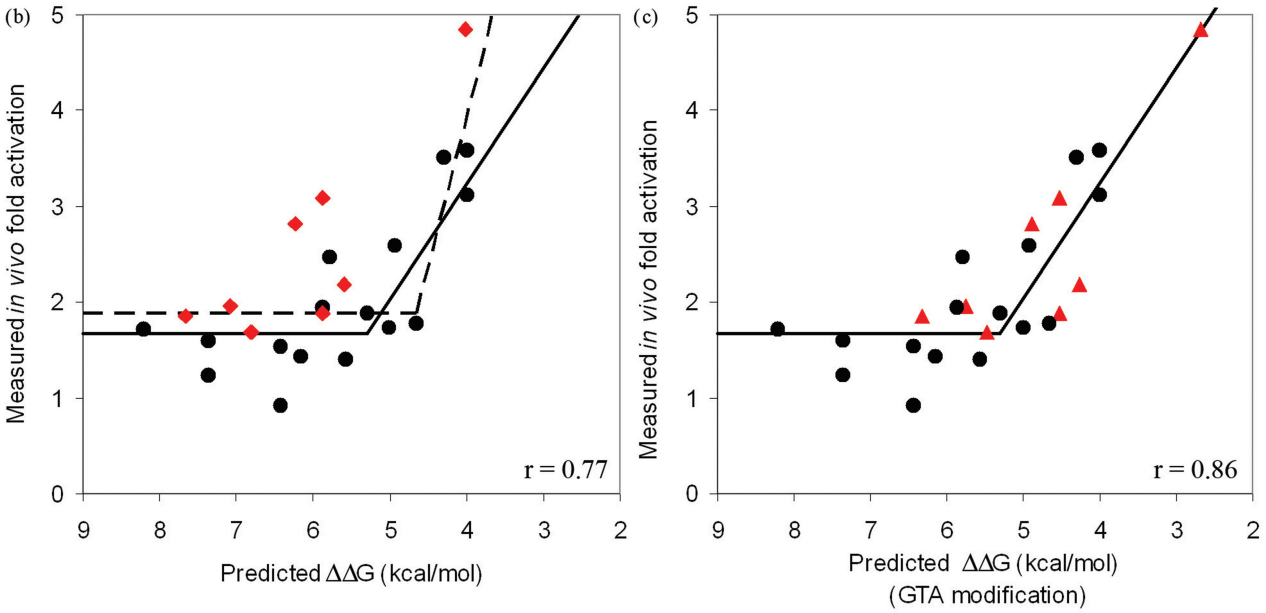

Figure 2. Predicted binding energies are highly correlated with *in vivo* activity in a B2H assay. Twenty-seven three-module ZFPs were designed by modular assembly to span a broad range of predicted binding affinities. (**a**) DNA recognition helix sequences, DNA sequence targets, predicted energies, measured fold-activation in the B2H assay, and standard error of the mean are listed for each construct. Entries are sorted from lowest to highest predicted ΔΔG. Constructs marked with an asterisk were also tested *in vitro* (Figure 4). (**b**) ZFP activities in the B2H assay are plotted versus predicted energies. The two constructs with highest predicted affinities were toxic to their host cells and therefore could not be included. Points shown as red diamonds correspond to proteins containing the GTA-specific QSSSLVR module (see text). Best-fit lines from a segmental linear regression model using all points (dashed line, $r = 0.77$), or excluding red points (solid line, $r = 0.86$) are shown. (**c**) Same as (b), except that values indicated by red triangles were adjusted assuming a binding affinity of 2.5 nM, rather than 25 nM, for the GTA-specific QSSSLVR module; this increases the correlation coefficient to 0.86 (see text for details).

Table 1. ZFP variants that differ in the middle (F2) position bind targets with variable affinities

	Helix N- to -C	Target 5′–3′	Affinity (K_d, nM)
Strong	QSSNLVR	GAA	0.5
	RSDHLTT	TGG	0.5
	RSDNLVR	GAG	1
	QSGDLRR	GCA	2
	TSGNLVR	GAT	3
	DPGNLVR	GAC	3
	QRAHLER	GGA	3
	TSGSLVR	GTT	5
	RSDKLTR	GGG	6
	RSDDLVR	GCG	9
Moderate	TSGHLVR	GGT	15
	RSDELVR	GTG	15
	QSSSLVR	GTA	25
Weak	DPGHLVR	GGC	40
	DPGALVR	GTC	40
	TSGELVR	GCT	65
	DCRDLAR	GCC	80

The data in this table were reported by Segal *et al.* (15). Each ZFD in the F2 position was selected to bind a particular target triplet. The F1 and F3 modules (derived from Zif268) were the same in each construct. A binding affinity constant for each ZFP variant was determined using an EMSA. Here, modules are classified based on the affinity of the ZFPs for their cognate target sites (*Strong*, *Moderate*, Weak). Three modules from each class were chosen to construct 27 diverse three-module ZFPs (Table 2).

Table 2. Single module substitutions in ZFPs alter target affinity

Position Varied	ZFP No.	F1 Helix	F2 Helix	F3 Helix	Fold Activation
1	**7**	RSDNLVR	DPGHLVR	TSGNLVR	3.11
	16	QSSSLVR	DPGHLVR	TSGNLVR	1.88
	25	TSGELVR	DPGHLVR	TSGNLVR	1.54
	8	RSDNLVR	DPGALVR	TSGHLVR	2.59
	17	QSSSLVR	DPGALVR	TSGHLVR	1.69
	26	TSGELVR	DPGALVR	TSGHLVR	1.59
	9	RSDNLVR	TSGELVR	DPGALVR	2.47
	18	QSSSLVR	TSGELVR	DPGALVR	1.85
	27	TSGELVR	TSGELVR	DPGALVR	1.71
2	**10**	RSDELVR	TSGSLVR	TSGSLVR	1.77
	13	RSDELVR	QSSSLVR	TSGSLVR	2.19
	11	RSDELVR	TSGSLVR	RSDELVR	1.89
	14	RSDELVR	QSSSLVR	RSDELVR	2.81
	12	TSGHLVR	TSGSLVR	TSGELVR	1.43
	15	TSGHLVR	QSSSLVR	TSGELVR	1.96
3	**1**	TSGSLVR	RSDNLVR	RSDNLVR	Toxic
	2	TSGSLVR	RSDNLVR	QSSSLVR	4.88
	3	TSGSLVR	RSDNLVR	DPGHLVR	3.51
	4	TSGNLVR	TSGHLVR	RSDNLVR	Toxic
	5	TSGNLVR	TSGHLVR	RSDELVR	1.71
	6	TSGNLVR	TSGHLVR	DPGHLVR	1.41
	19	DPGHLVR	TSGNLVR	RSDNLVR	3.58
	20	DPGHLVR	TSGNLVR	QSSSLVR	3.09
	21	DPGHLVR	TSGNLVR	TSGELVR	0.92
	22	DPGALVR	RSDELVR	TSGSLVR	1.95
	23	DPGALVR	RSDELVR	QSSSLVR	1.69
	24	DPGALVR	RSDELVR	TSGELVR	1.23

Individual ZFDs, represented by their DNA recognition helix, are shaded to indicate their affinity class (*Strong*, *Moderate*, Weak, see Table 1). For each subgroup (demarcated by horizontal lines), modules in two positions were held constant while the position indicated in the leftmost column was varied. Fold activation denotes performance of the ZFP in the B2H assay. Toxic refers to the poor growth of *E. coli* cultures observed when cells expressed certain ZFPs.

preventing analysis of these constructs. Several models describing the relationship between predicted and measured activity were evaluated, with segmental linear regression providing the best fit ($r = 0.77$; Figure 2b, dashed line). Inspection of the data revealed that the GTA-specific module (QSSSLVR) was present in most ZFPs that exhibited significantly greater activation than predicted (Figure 2b, red diamonds). Excluding ZFPs containing this module from the analysis increased the correlation coefficient to 0.86 (Figure 2b, solid line).

The predictions described above relied on published *in vitro* binding affinities for ZFPs in which modules were evaluated in a fixed context (15) to estimate binding contributions of individual modules. In an alternate approach, we predicted ZFP performance by solving individual module contributions as component variables of a system of linear equations. Briefly, in constructing the 27 different three-finger proteins, nine ZFDs were used approximately 8–10 times (approximately three times at each of the possible three positions, Table 1). Assuming that the energy contributions of individual ZFDs in a ZFP are additive, the B2H activity of each ZFP was considered to result from its particular combination of modules (Supplementary Figure 1). Individual module contributions were calculated for each ZFP using a leave-one-out linear system solution. Expected *lacZ* activation in the B2H assay for each of the ZFPs was then predicted by summing individual module contributions. As shown in Figure 3, expected levels of activation computed in this manner were highly correlated with actual B2H activity measurements ($r = 0.86$).

The energy contributions computed using a system of linear equations to analyze *in vivo* activity data from the B2H assay indicate that the GTA-specific QSSSLVR module binds with higher affinity than previous K_d estimates. This is consistent with our conclusion based on inspection of energies computed from *in vitro* binding constants (Figure 2b). We estimated a new value for this module by calculating the K_d that optimizes the correlation of predicted energies with the B2H data. This approach resulted in an estimated K_d of 2.5 nM for this module, 10-fold lower than the previously reported value of 25 nM (15). Incorporating this new estimate improved correlation between the *in vitro* energy model and *in vivo* fold activation data ($r = 0.86$, Figure 2c).

To directly evaluate the effects of individual module affinities on *in vivo* performance, sets of related ZFPs designed to vary at a single module position were analyzed for differences in B2H activity (Table 2). For all three sets of ZFPs in which the F1 position was varied (while F2 and F3 were fixed), the greatest *in vivo* activity was observed when the F1 position contained a high affinity module; the least activity was observed with a low affinity module in this position. The same trend was observed for all four

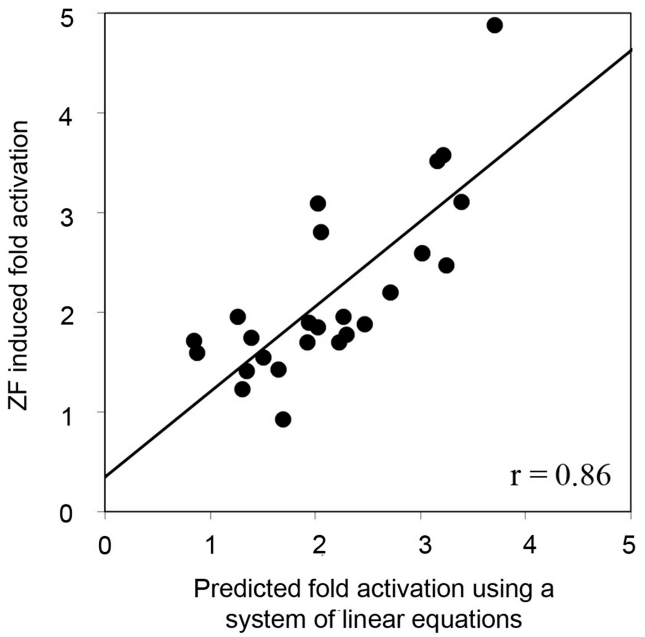

Figure 3. ZFDs contribute additively to B2H activity, independent of context and position. For each ZF protein, the expected contribution to B2H activity from each of its component modules was estimated by solving a system of linear equations representing the other 24 proteins (see text). Comparison of actual versus predicted B2H activity (expressed as relative fold-activation in the B2H assay) reveals a high correlation ($r = 0.86$).

groups in which the F3 position was varied while the F1 and F2 fingers were fixed. For sets in which the F2 position was varied, only one strong module (TSGSLVR) and one moderate affinity module (QSSSLVR) were tested. In these cases, the moderate affinity module outperformed the high affinity module. These results suggest that the effect of single module substitutions on relative binding affinity can be predicted reliably in most cases.

In summary, three lines of analysis: (i) predictions based on *in vitro* binding constants for modules in a fixed context, (ii) predictions derived from a system of linear equations based on *in vivo* performance and (iii) analysis of the effects of various single finger substitutions *in vivo*, demonstrate that *in vivo* performance for ZFPs can be predicted based on DNA-binding affinities of individual ZFDs.

In vitro DNA binding affinities of ZFPs are highly correlated with predicted binding energies

Our success in estimating the activities of ZFPs in the B2H assay suggested that our scoring scheme could be applied more generally to predict *in vitro* ZFP affinities. To test whether activation measured in the B2H assay directly reflects DNA binding affinity for the desired target site, 9 of the 27 engineered proteins, along with a control Zif268 protein, were chosen for *in vitro* binding affinity measurements (Figure 4). K_d values were determined using fluorescence anisotropy (FA), a rapid and reproducible solution-based DNA binding assay that allows computation of the bound fraction of a fluorescently labeled ligand, based on the decrease in its rotational velocity due to binding (33,34).

As shown in Figure 5, binding affinity constants determined by FA were highly correlated with predicted energies. The two ZF proteins with highest predicted affinities were toxic to bacterial cells, prohibiting purification of sufficient quantities of protein for *in vitro* analysis. Energies computed based on previously published *in vitro* affinity measurements for modules in a fixed context (15) were proportional to the log of K_d's measured in our experiments ($r = 0.91$) (Figure 5a). As before, assuming a K_d of 2.5 nM for the QSSSLVR module significantly improved the correlation ($r = 0.97$). Predicted *in vivo* activation levels generated by the leave-one-out linear system method were also highly correlated with experimentally determined binding constants ($r = 0.93$; Figure 5b). Thus, results obtained using a rapid and reliable spectroscopic method suggest that ZFP binding affinities measured *in vitro* generally correspond to results obtained *in vivo* using the B2H system. This demonstrates that our rule-based strategy can be used to predict ZFP DNA binding affinity.

A binding energy threshold for ZFP function *in vivo*

To evaluate the generality of this rule-based approach, we calculated predicted energies for another set of modularly assembled ZFPs that had been previously evaluated using the B2H system (25). From 168 modularly assembled ZFPs, we selected all ZFPs comprising GNN or TGG modules for which published *in vitro* DNA binding affinity constants are available [measured in the F2 position of the standard Zif268 variant backbone (15)]. As shown in Figure 6a, based on a segmental linear regression model, binding energies for 24 of these 26 ZFPs are highly correlated ($r = 0.80$) with reported B2H activity measurements. These results are also in excellent agreement with the results described above and shown in Figure 2b, although slightly higher activation levels were uniformly observed in the latter experiments. Notably, both sets of experiments identify a $\Delta\Delta G$ of $\sim$5 kcal/mol (corresponding to a K_d of $\sim$100 nM) as the threshold for zinc-finger function *in vivo* (in bacterial cells). We also used the scoring function generated from the B2H experiments performed by us (and shown in Figure 2c) to predict B2H activity for the 24 ZFPs evaluated by Ramirez *et al*. (25). Again, the predicted and measured fold-activation scores were in close agreement, with a correlation coefficient of 0.79 (Figure 6b). Taken together, these results suggest that the scoring function developed and evaluated may be generally applicable to ZFPs assembled using the Barbas lab GNN modules.

DISCUSSION

Using a rule-based strategy that combines experimentally determined binding energies of individual ZFDs, we were able to compute binding energies for ZFPs made from a particular set of well-characterized GNN modules (15). We also showed that these predicted binding energies are in excellent agreement ($r = 0.91$; Figure 5a) with binding affinity constants measured directly *in vitro*. Furthermore, we showed a strong correlation between these computed

(a)

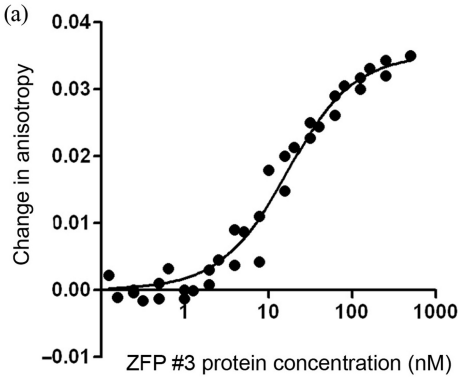

(b)

ID#	Predicted ΔΔG	K_d (nM)
1	2.15	Toxic
19	4.00	Toxic
2	4.02	7.8
3	4.29	14.2
13	5.60	26.3
20	5.87	33.1
11	5.30	247.0
21	6.43	704.0
27	8.22	7466.0

Figure 4. Determining binding affinity constants using fluorescence anisotropy. (**a**) A representative *in vitro* binding isotherm obtained using FA. Data points for each ZFP were collected using three separate purified protein preparations, each assayed for binding activity on a different day. Curve fitting was performed using **P**rism. (**b**) K_d values for seven modularly assembled ZFPs, determined in FA experiments. Note that two ZFPs were toxic to host cells, preventing purification of proteins in quantities required for *in vitro* analysis.

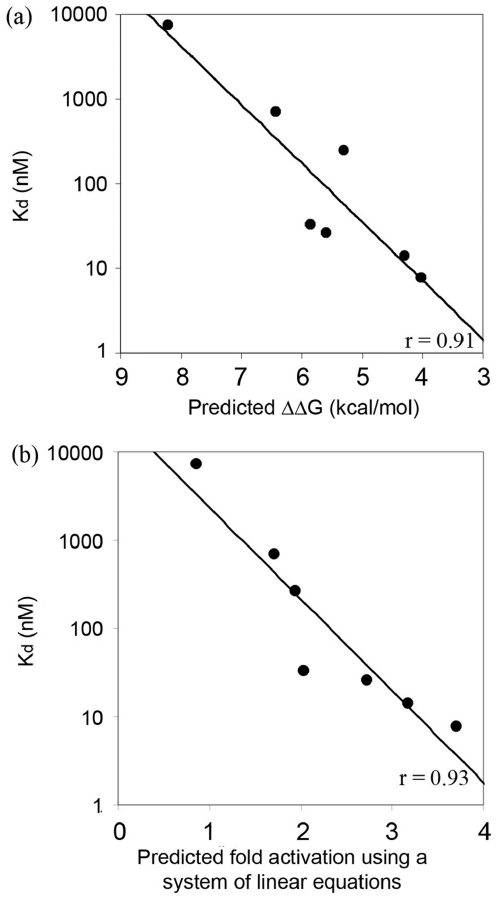

Figure 5. *In vitro* affinity constants for ZFPs are highly correlated with predictions. Using affinity constants for seven ZFPs determined by FA (Figure 4b), log(*K*d) is plotted against: (**a**) predicted energy, expressed as ΔΔG in kcal/mol ($r = 0.91$) and (**b**) predicted B2H activity based on a leave-one-out system of linear equations analysis ($r = 0.93$).

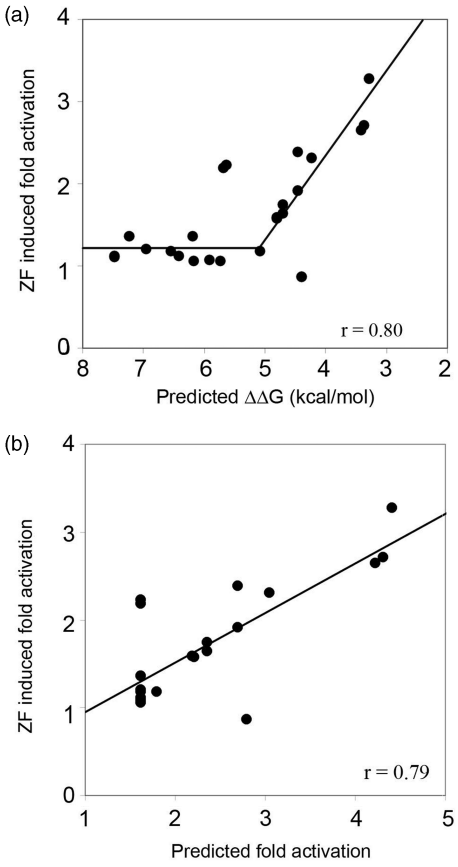

Figure 6. Predicted ZFP performance agrees with *in vivo* activity for an independently generated set of ZFPs. Data shown are for 24 of 26 ZFPs containing characterized GNN or TGG modules, constructed and evaluated by Ramirez *et al.* (25) (**a**) A segmental linear regression model provides an excellent fit of *in vivo* ZF-induced fold activation measured in the B2H assay with predicted binding energies (r = 0.80). (**b**) ZF-induced fold activation values measured in the B2H assay for 24 ZFPs from Ramirez *et al.* (25) are also highly correlated ($r = 0.79$) with predicted fold-activation levels calculated based on a scoring function derived from the segmental linear regression model fit for the 25 ZFPs shown in Figure 2a (see text for details). Note: predictions for 2 of 26 ZFPs containing characterized GNN or TGG modules from Ramirez *et al.* (25) were considered outliers (values were outside the range included in these graphs); they were not included in the regression analysis.

binding energies and ZFP activities in a B2H system for two different sets of modularly assembled three-finger ZFPs. This is an important advance because a ZFP that lacks activity in the B2H system will also have a high

probability of failing to function as a ZFN in human cells (24–26). Thus, using only our scoring method, researchers can now identify target sites that will have a high probability of failing to yield functional zinc-finger arrays by the method of modular assembly. Our rule-based strategy will thus allow researchers to focus their modular assembly efforts on a smaller number of target sites with a higher probability of success.

We believe that our results also provide one potential explanation for the discrepancy between the overwhelming success rates for a previous *in vitro* report (35) and the low *in vivo* success rates observed for ZFPs in the recent study of Ramirez *et al*. (25): many of the modules used to perform modular assembly likely possess low affinities. Our data suggest, in fact, that 30–50% of potential three-finger ZFPs made wholly from the Barbas GNN modules will fail to function in the B2H system, a result in agreement with the recently published results of Ramirez *et al*. (25).

Although our results demonstrate that the energy contributions of individual ZFDs in a ZFP array are additive, we also believe they lend additional support to the notion that context is an important parameter that should be accounted for when engineering multi-finger ZFPs (i.e. that one single ZFD module will not always be optimal or adequate for recognition of its cognate 3-bp subsite in different multi-finger ZFP contexts). For example, our data show that although a weak finger will sometimes be found in a nonfunctional ZFP array (if it is joined together with other weak affinity ZFDs), it will also sometimes be found in functional arrays when paired with stronger affinity ZFDs. In addition, our data show that although strong fingers will sometimes be found in functional ZFPs, they can be found in nonfunctional ZFPs. Furthermore, the use of three strong fingers in a ZFP can lead to toxicity in *E. coli* cells. Although the precise mechanism of this toxicity is unclear, a reasonable hypothesis is that excessively high affinity leads to binding to related but off-target sequences with sufficient affinity to cause biological consequences (essentially, excessive affinity leading to problems of specificity). Thus, our data further re-enforce the ideas that individual ZFDs do not function completely independently and that the specific attributes of neighboring fingers do matter in the context of engineering a multi-finger ZFP.

The importance of context-dependent effects also suggests that identification of additional ZFDs with variable affinities for GNN triplets may be needed if the efficiency of modular assembly is to be improved. If such ZFDs were available, it might be possible to achieve higher success rates for modular assembly by creating several ZFPs for a given target site so as to identify a combination that balances affinities (and presumably, specificities) of its component ZFDs. A related point is that our findings also suggest one possible reason why more complex selection-based methods that account for context-dependent effects [e.g. the OPEN method recently described by Joung and colleagues (26,32)] may be more successful than modular assembly: these methods are able to balance the overall affinity and specificity of the final ZFP array by identifying optimal combinations from various ZFDs with a range of affinities and specificities for their target 3-bp subsites.

The strong correlations among predicted binding energies, *in vivo* activities, and *in vitro* binding affinity constants for the ZFPs analyzed in this work suggests that our rule-based approach might be extended to evaluate arrays assembled using GNN modules from other sources (17,19) and non-GNN modules. We have not yet evaluated such modules, but our work demonstrates two ways this could be achieved: (i) by directly measuring *in vitro* binding constants for modules in the F2 position of a standardized ZFP framework and (ii) by computing individual module contributions to ZFP binding as component variables of a system of linear equations that describe their activities (measured *in vivo* in this work, but *in vitro* binding constants could also be used). The energy scoring scheme proposed here will allow researchers to determine whether a modular assembly strategy is likely to be feasible for specific targets of interest, based on currently available well-characterized modules, or whether an alternative selection-based engineering strategy should be considered.

A recent study on the use of ZFNs for homologous recombination cited lack of specificity as a primary determinant of ZFN-mediated toxicity in human cells (24). A likely mechanism for ZFN-induced toxicity is through binding to genomic sequences similar to the desired target sequence. As noted above, we observed toxicity in bacterial cells for several ZFPs, even in the absence of a fused nuclease domain, suggesting that ZFP binding to certain sites in genomic DNA can be toxic, particularly for high affinity ZFPs. Although this is the first published report of such toxicity in bacterial cells that we are aware of, it has been observed previously for several other sites (Joung,J.K. unpublished data). However, bacterial expression of ZFPs with affinities in the pM range, with no toxic effects, has also been reported (19,36,37). High-throughput chip or microfluidics-based DNA binding experiments (38–41) could be used to obtain affinity and specificity data for virtually every possible target site for a given ZFP, providing additional insight into ZFP-induced toxicity and into the fundamental rules that govern the affinity and specificity of DNA recognition by zinc-finger DNA binding proteins.

A correlation between ZFP binding constants measured *in vitro* and functional activity measured *in vivo* has also been observed by others using different reporter systems (37). A similar degree of correlation was observed using the B2H system in our study (Supplementary Figure 2). Our results further demonstrate that measurable ZFP activity in an *in vitro* binding assay does not necessarily translate into adequate function *in vivo*, in agreement with Beerli *et al*. (42). However, the energy threshold we determined for ZFP activity *in vivo*, using B2H assays, corresponds to a K_d of $\sim$100 nM, and thus differs from the estimated threshold K_d of $\sim$10 nM reported as the minimum affinity necessary for ZFP function in mammalian cells (42). The significance of this difference between thresholds determined in bacterial and mammalian cells is difficult to evaluate, given that functional assays and K_d measurements were performed in

different laboratories using different assays and with ZFPs containing different numbers of fingers.

Stormo and colleagues (43–47) have shown that the DNA-binding specificity of ZFPs can be effectively predicted from additive energy contributions of individual residues that make base-specific contacts with target site nucleotides. Our results complement this idea by demonstrating that the affinity of ZFPs also can be predicted, using affinity data for component modules. Our application of the binding energy additivity concept differs somewhat from that used by Stormo to predict specificity in that it assumes additivity of energy contributions at the individual finger rather than individual residue level. Also, our approach implicitly includes energetic contributions of residues that are not directly involved in base contacts (e.g. phosphate contacts), as well as energetic contributions resulting from context-dependent effects that presumably occur among recognition helix residues within each finger.

The apparent simplicity of modular assembly has contributed to the current focus on C_2H_2 ZFDs as the domains of choice for designing custom DNA binding proteins. Our results make it possible, for the first time, to reliably identify prospective binding sites that are unlikely to yield functional ZFDs by modular assembly using a set of GNN-specific finger modules. The rule-based strategy presented here can provide accurate guidance for both *in vitro* binding affinities and *in vivo* functionality for engineered ZFPs by computing energy contributions of individual ZFDs. We have updated the Zinc Finger Targeter (ZiFiT) web server (http://bindr.gdcb.iastate.edu/ZiFiT) (48) so that it now provides users with a list of potential ZFP-target site pairs for a desired genomic sequence, scored according to the procedures developed and validated in this work.

SUPPLEMENTARY DATA

Supplementary Data are available at NAR Online.

ACKNOWLEDGEMENTS

We thank members of our groups and colleagues, especially Fengli Fu, Deepak Reyon, David Wright, Ronnie Winfrey, Ben Lewis, Bob Farnham, Abd Elhamid Azzaz, Les Miller, Gaya Amarasinghe and Vasant Honavar and the referees for their helpful suggestions and valuable feedback. We also thank Guru Rao for the use of his spectrophotometer.

FUNDING

National Institutes of Health (GM066387 to D.D.); National Science Foundation (DBI0501678 to D.F.V.); National Institutes of Health (GM069906 and GM078369 to J.K.J.); and graduate research assistantships provided by United States Department of Agriculture (MGET 2001-52100-11506, NSF IGERT0504304 and ISU's Center for Integrated Animal Genomics (CIAG). Funding for open access charge: National Science Foundation (DBI0501678).

Conflict of interest statement. None declared.

REFERENCES

1. Durai,S., Mani,M., Kandavelou,K., Wu,J., Porteus,M.H. and Chandrasegaran,S. (2005) Zinc finger nucleases: custom-designed molecular scissors for genome engineering of plant and mammalian cells. *Nucleic Acids Res.*, **33**, 5978–5990.
2. Klug,A. (2005) Towards therapeutic applications of engineered zinc finger proteins. *FEBS Lett.*, **579**, 892–894.
3. Porteus,M.H. and Carroll,D. (2005) Gene targeting using zinc finger nucleases. *Nat. Biotechnol.*, **23**, 967–973.
4. Wu,J., Kandavelou,K. and Chandrasegaran,S. (2007) Custom-designed zinc finger nucleases: what is next? *Cell. Mol. Life Sci.*, **64**, 2933–2944.
5. Cathomen,T. and Joung,J.K. (2008) Zinc-finger nucleases: the next generation emerges. *Mol. Ther.*, **16**, 1200–1207.
6. Desjarlais,J.R. and Berg,J.M. (1993) Use of a zinc-finger consensus sequence framework and specificity rules to design specific DNA binding proteins. *Proc. Natl Acad. Sci. USA*, **90**, 2256–2260.
7. Jamieson,A.C., Wang,H. and Kim,S.H. (1996) A zinc finger directory for high-affinity DNA recognition. *Proc. Natl Acad. Sci. USA*, **93**, 12834–12839.
8. Beerli,R.R., Segal,D.J., Dreier,B. and Barbas,C.F. 3rd. (1998) Toward controlling gene expression at will: specific regulation of the erbB-2/HER-2 promoter by using polydactyl zinc finger proteins constructed from modular building blocks. *Proc. Natl Acad. Sci. USA*, **95**, 14628–14633.
9. Wolfe,S.A., Nekludova,L. and Pabo,C.O. (2000) DNA recognition by Cys2His2 zinc finger proteins. *Annu. Rev. Biophys. Biomol. Struct.*, **29**, 183–212.
10. Pabo,C.O., Peisach,E. and Grant,R.A. (2001) Design and selection of novel Cys2His2 zinc finger proteins. *Annu. Rev. Biochem.*, **70**, 313–340.
11. Segal,D.J. (2002) The use of zinc finger peptides to study the role of specific factor binding sites in the chromatin environment. *Methods*, **26**, 76–83.
12. Pavletich,N.P. and Pabo,C.O. (1991) Zinc finger-DNA recognition: crystal structure of a Zif268-DNA complex at 2.1 A. *Science*, **252**, 809–817.
13. Elrod-Erickson,M., Rould,M.A., Nekludova,L. and Pabo,C.O. (1996) Zif268 protein-DNA complex refined at 1.6 A: a model system for understanding zinc finger-DNA interactions. *Structure*, **4**, 1171–1180.
14. Miller,J.C. and Pabo,C.O. (2001) Rearrangement of side-chains in a Zif268 mutant highlights the complexities of zinc finger-DNA recognition. *J. Mol. Biol.*, **313**, 309–315.
15. Segal,D.J., Dreier,B., Beerli,R.R. and Barbas,C.F. 3rd. (1999) Toward controlling gene expression at will: selection and design of zinc finger domains recognizing each of the 5'-GNN-3' DNA target sequences. *Proc. Natl Acad. Sci. USA*, **96**, 2758–2763.
16. Wolfe,S.A., Greisman,H.A., Ramm,E.I. and Pabo,C.O. (1999) Analysis of zinc fingers optimized via phage display: evaluating the utility of a recognition code. *J. Mol. Biol.*, **285**, 1917–1934.
17. Liu,Q., Xia,Z., Zhong,X. and Case,C.C. (2002) Validated zinc finger protein designs for all 16 GNN DNA triplet targets. *J. Biol. Chem.*, **277**, 3850–3856.
18. Dreier,B., Beerli,R.R., Segal,D.J., Flippin,J.D. and Barbas,C.F. 3rd. (2001) Development of zinc finger domains for recognition of the 5'-ANN-3' family of DNA sequences and their use in the construction of artificial transcription factors. *J. Biol. Chem.*, **276**, 29466–29478.
19. Bae,K.H., Kwon,Y.D., Shin,H.C., Hwang,M.S., Ryu,E.H., Park,K.S., Yang,H.Y., Lee,D.K., Lee,Y., Park,J. *et al.* (2003) Human zinc fingers as building blocks in the construction of artificial transcription factors. *Nat. Biotechnol.*, **21**, 275–280.
20. Dreier,B., Fuller,R.P., Segal,D.J., Lund,C.V., Blancafort,P., Huber,A., Koksch,B. and Barbas,C.F. 3rd. (2005) Development of zinc finger domains for recognition of the 5′-CNN-3′ family DNA sequences and their use in the construction of artificial transcription factors. *J. Biol. Chem.*, **280**, 35588–35597.

21. Alwin,S., Gere,M.B., Guhl,E., Effertz,K., Barbas,C.F. 3rd., Segal,D.J., Weitzman,M.D. and Cathomen,T. (2005) Custom zinc-finger nucleases for use in human cells. *Mol. Ther*., **12**, 610–617.
22. Beumer,K., Bhattacharyya,G., Bibikova,M., Trautman,J.K. and Carroll,D. (2006) Efficient gene targeting in Drosophila with zinc-finger nucleases. *Genetics*, **172**, 2391–2403.
23. Segal,D.J., Crotty,J.W., Bhakta,M.S., Barbas,C.F. 3rd. and Horton,N.C. (2006) Structure of Aart, a designed six-finger zinc finger peptide, bound to DNA. *J. Mol. Biol*., **363**, 405–421.
24. Cornu,T.I., Thibodeau-Beganny,S., Guhl,E., Alwin,S., Eichtinger,M., Joung,J.K. and Cathomen,T. (2008) DNA-binding specificity is a major determinant of the activity and toxicity of zinc-finger nucleases. *Mol. Ther*., **16**, 352–358.
25. Ramirez,C.L., Foley,J.E., Wright,D.A., Muller-Lerch,F., Rahman,S.H., Cornu,T.I., Winfrey,R.J., Sander,J.D., Fu,F., Townsend,J.A. *et al*. (2008) Unexpected failure rates for modular assembly of engineered zinc fingers. *Nat. Methods*, **5**, 374–375.
26. Maeder,M.L., Thibodeau-Beganny,S., Osiak,A., Wright,D.A., Anthony,R.M., Eichtinger,M., Jiang,T., Foley,J.E., Winfrey,R.J., Townsend,J.A. *et al*. (2008) Rapid ''open-source'' engineering of customized zinc-finger nucleases for highly efficient gene modification. *Mol. Cell*, **31**, 294–301.
27. Wright,D.A., Thibodeau-Beganny,S., Sander,J.D., Winfrey,R.J., Hirsh,A.S., Eichtinger,M., Fu,F., Porteus,M.H., Dobbs,D., Voytas,D.F. *et al*. (2006) Standardized reagents and protocols for engineering zinc finger nucleases by modular assembly. *Nat. Protoc*., **1**, 1637–1652.
28. Ryder,S.P., Frater,L.A., Abramovitz,D.L., Goodwin,E.B. and Williamson,J.R. (2004) RNA target specificity of the STAR/GSG domain post-transcriptional regulatory protein GLD-1. *Nat. Struct. Mol. Biol*., **11**, 20–28.
29. Seidman, C.E. (1997) Transformation using calcium chloride. In Ausubel, F.M. (ed), *Current Protocols in Molecular Biology*, Vol. I Unit 1.8. John Wiley & Son, Inc., New York.
30. Lundblad,J.R., Laurance,M. and Goodman,R.H. (1996) Fluorescence polarization analysis of protein-DNA and protein-protein interactions. *Mol. Endocrinol*., **10**, 607–612.
31. LiCata,V.J. and Wowor,A.J. (2008) Applications of fluorescence anisotropy to the study of protein-DNA interactions. *Methods Cell Biol*., **84**, 243–262.
32. Hurt,J.A., Thibodeau,S.A., Hirsh,A.S., Pabo,C.O. and Joung,J.K. (2003) Highly specific zinc finger proteins obtained by directed domain shuffling and cell-based selection. *Proc. Natl Acad. Sci. USA*, **100**, 12271–12276.
33. Veprintsev,D.B. and Fersht,A.R. (2008) Algorithm for prediction of tumour suppressor p53 affinity for binding sites in DNA. *Nucleic Acids Res*., **36**, 1589–1598.
34. Hayouka,Z., Rosenbluh,J., Levin,A., Maes,M., Loyter,A. and Friedler,A. (2008) Peptides derived from HIV-1 Rev inhibit HIV-1 integrase in a shiftide mechanism. *Biopolymers*, **90**, 481–487.
35. Segal,D.J., Beerli,R.R., Blancafort,P., Dreier,B., Effertz,K., Huber,A., Koksch,B., Lund,C.V., Magnenat,L., Valente,D. *et al*. (2003) Evaluation of a modular strategy for the construction of novel polydactyl zinc finger DNA-binding proteins. *Biochemistry*, **42**, 2137–2148.
36. Yang,W.P., Wu,H. and Barbas,C.F. 3rd. (1995) Surface plasmon resonance based kinetic studies of zinc finger-DNA interactions. *J. Immunol. Methods*, **183**, 175–182.
37. Kang,J.S. (2007) Correlation between functional and binding activities of designer zinc-finger proteins. *Biochem. J*., **403**, 177–182.
38. Bulyk,M.L. (2006) DNA microarray technologies for measuring protein-DNA interactions. *Curr. Opin. Biotechnol*., **17**, 422–430.
39. Berger,M.F., Philippakis,A.A., Qureshi,A.M., He,F.S., Estep,P.W. 3rd and Bulyk,M.L. (2006) Compact, universal DNA microarrays to comprehensively determine transcription-factor binding site specificities. *Nat. Biotechnol*., **24**, 1429–1435.
40. Maerkl,S.J. and Quake,S.R. (2007) A systems approach to measuring the binding energy landscapes of transcription factors. *Science*, **315**, 233–237.
41. Berger,M.F., Badis,G., Gehrke,A.R., Talukder,S., Philippakis,A.A., Pena-Castillo,L., Alleyne,T.M., Mnaimneh,S., Botvinnik,O.B., Chan,E.T. *et al*. (2008) Variation in homeodomain DNA binding revealed by high-resolution analysis of sequence preferences. *Cell*, **133**, 1266–1276.
42. Beerli,R.R., Dreier,B. and Barbas,C.F. 3rd. (2000) Positive and negative regulation of endogenous genes by designed transcription factors. *Proc. Natl Acad. Sci. USA*, **97**, 1495–1500.
43. Stormo,G.D. and Fields,D.S. (1998) Specificity, free energy and information content in protein-DNA interactions. *Trends Biochem. Sci*., **23**, 109–113.
44. Benos,P.V., Bulyk,M.L. and Stormo,G.D. (2002) Additivity in protein-DNA interactions: how good an approximation is it? *Nucleic Acids Res*., **30**, 4442–4451.
45. Benos,P.V., Lapedes,A.S. and Stormo,G.D. (2002) Probabilistic code for DNA recognition by proteins of the EGR family. *J. Mol. Biol*., **323**, 701–727.
46. Liu,J. and Stormo,G.D. (2005) Quantitative analysis of EGR proteins binding to DNA: assessing additivity in both the binding site and the protein. *BMC Bioinformatics*, **6**, 176.
47. Liu,J. and Stormo,G.D. (2008) Context-dependent DNA recognition code for C2H2 zinc-finger transcription factors. *Bioinformatics*, **24**, 1850–1857.
48. Sander,J.D., Zaback,P., Joung,J.K., Voytas,D.F. and Dobbs,D. (2007) Zinc Finger Targeter (ZiFiT): an engineered zinc finger/target site design tool. *Nucleic Acids Res*., **35**, W599–W605.